IEEE Access
Multidisciplinary | Rapid Review | Open Access Journal

Received March 26, 2021, accepted April 11, 2021, date of publication April 14, 2021, date of current version April 23, 2021.

Digital Object Identifier 10.1109/ACCESS.2021.3073222

Impact Analysis and Calibration Methods of Excitation Errors for Phased Array Antennas

GUOLONG HE, XIN GAO, AND RENTIAN ZHANG
Beijing Institute of Tracking and Telecommunication Technology, Beijing 100094, China
Corresponding author: Guolong He (heguolong@alumni.sjtu.edu.cn)

ABSTRACT Phased array antennas have played a very important role in many different areas and applications. It requires precise excitation of each antenna element by various synthesis techniques to obtain desired array pattern features. However, due to reasons such as manufacturing imperfections, component aging, and temperature variation, the realistic antenna element excitation inevitably differs from their expected values in practice. This paper presents a tutorial-like review to deal with excitation errors for phased array antennas. Two kinds of analysis methods, probabilistic methods and interval arithmetic (IA) based methods, are presented to evaluate the effects of excitation errors for phased array antennas. State-of-the-art calibration methods along with various signal processing techniques are reviewed, their advantages and challenges are discussed in a comparative manner. Some other common errors and open research directions are also presented.

INDEX TERMS Phased array antenna, excitation error, interval arithmetic, array calibration.

I. INTRODUCTION

The first phased array antenna was invented around the turn of the 20th century with mechanical rotation to steer the beam [1]. It was not until World War II that remarkable progress such as controlled phase shifters were made, which began to replace the original mechanical antenna steering. With the military need for large missile warning and space surveillance radars during the cold war, phased array antenna technologies were fast developed and quickly played an important role in defense areas like radar, sonar, navigation, and wireless communications [2], [3]. At that time, the phased array antennas utilized passive architecture with a centralized high-power transmit amplifier and receiver. However, the phased array antennas have undergone a steady evolution over the years. Thanks to advancements in GaAs microwave circuits during the 1980s, active electronically scanned arrays with analog beamforming architecture became very popular, where each element has its own full independent transmit/receive (T/R) module. By the end of the 1990s, experiments and implements with hybrid analog-digital beamforming architecture were also extensively investigated and gradually became mature [4]–[6].

After entering into the 21st century, with element level digitization and fully digital beamforming (DBF) architecture, phased array antennas have gained a much wider range of improvements in both capability and performance. With the important breakthrough with silicon(Si)-based phased array technology, it has been driven to a point affordable for a huge number of civil and commercial applications, including not only 5G communication and wireless localization, but also medical imaging, autonomous driving, and Internet of Things (IOT) that enrich our daily lives [7]–[10]. Nowadays, Si-based phased array technologies have been reported covering in a very wide frequency range from millimeter-wave (mm-wave) to sub-millimeter-wave band, and even in terahertz (THz) frequency band [11]. These modern applications with increasing working frequency impose much more stringent requirements on phased array antennas, adding significant constraints to the size, cost, complexity, and weight, and most importantly, performance of the array.

By amplitude tapering and phase control of antenna elements, phased array antennas can agilely steer the beam, control the sidelobe levels (SLLs), and present the nulls on the interfere directions conveniently [12]–[19]. This requires precise excitation of each antenna element by various synthesis techniques to obtain desired array pattern features, e.g., high directivity, low SLL, and null control. However, because

The associate editor coordinating the review of this manuscript and approving it for publication was Derek Abbott.

of mechanical manufacturing imperfections and circuit differences, phased array antennas show element to element variation. Moreover, due to component aging and temperature variation, the realistic antenna element excitations inevitably differ from their expected values in practice. These errors would cause array pattern distortion, gain degradation, worse SLL, and null drifts [20]–[23]. Therefore, knowledge about the impacts of the excitation errors and the corresponding calibration methods are of high importance for phased array antennas.

This paper aims to present a tutorial-like review of impact analysis and state-of-the-art calibration methods to overcome excitation errors for phased array antennas. Many methods have been proposed to analyze the impacts of excitation errors on array performance. These analysis methods fall into mainly two different types, probabilistic methods and interval arithmetic (IA) based methods. The probabilistic methods assume that the excitation errors follow some kind of probability distribution function (PDF) and treat this problem via statistical derivation [24]–[29]. They can provide simple closed-form expressions of the features of the array pattern by exploiting the central limit theorem. Although well established, statistical methods have not always guaranteed reliable confidence bounds, some extreme cases can still fall outside the bounds. On the contrary, IA based methods introduce intervals to represent the possible values of the element excitation including both amplitude and phase, and predict the array performance by its upper and lower bounds [30]–[40]. Thanks to the inclusion property of IA to deal with uncertainties, the determined bounds of antenna array pattern are finite and inclusive thus reliable. Moreover, with respect to standard time-consuming Monte Carlo (MC) based strategies, IA based methods allow analyzing the effects of array excitation errors by means of analytic expressions in a short time.

To compensate for the excitation errors as low as possible and maintain acceptable array performance, phased array antennas are required to be carefully calibrated before their deployments and during their work. These calibration methods vary from different systems and applications, either suitable for factory test or for in-field test [41]. Some methods such as the near-field scanning probe method and the peripheral fixed probe method require additional equipments [42], [42]–[60], while the mutual coupling method takes advantage of the inherent property of the phased array without the need for extra hardware [61]–[71]. For Si-based integrated phased array antenna, it's very common to design a dedicated coupling network that using transmission lines connected to each antenna element for periodic in-field calibration [22], [72]–[86]. Moreover, different trade-off strategies can be made between the complexity of measurement setup and signal processing requirements. Some calibration techniques characterize the antenna elements one by one, while some others can handle several calibrations simultaneously. Some calibration techniques require the calibration source and sink must be coherent, while some others require no such synchronization and can be done by amplitude or power only measurements.

Figure 1 illustrates the main topics and general flowchart of this paper, including analysis methods, calibration methods, and signal processing techniques of excitation errors for phased array antennas. The rest of this paper is organized as follows. First in Section 2, the mathematical model of excitation errors is introduced along with the probabilistic analysis methods. Then in Section 3, according to the geometry of the excitation error representation, three kinds of IA based methods are presented. Next, state-of-the-art calibration methods for phased array antennas are reviewed in Section 4, their advantages and challenges are discussed in a comparative manner. Some signal processing techniques for phased array calibration are also reviewed in Section 5. Two other common errors, position errors and quantization errors, are also discussed in Section 6. Then in Section 7, two open research directions are presented to encourage future research about phased array calibration. Finally, this paper is concluded in Section 8.

II. PROBABILISTIC METHODS FOR IMPACT ANALYSIS

A. THE MATHEMATICAL MODEL

Considering a phased array antenna with N isotropic elements, each element has the excitation amplitude $\{a_n\}$ and phase $\{p_n\}$, $n = 1,\ldots, N$. The array radiation pattern or the array factor $f(\theta, \phi)$ can be mathematically expressed as follows,

$$\begin{aligned} f(\theta,\phi) &= \sum_{n=1}^{N} f_n(\theta,\phi) \\ &= \sum_{n=1}^{N} a_n \exp[j(2\pi/\lambda\, \overrightarrow{k}\,(\theta,\phi)\cdot \overrightarrow{r_n} + p_n)] \\ &= \sum_{n=1}^{N} a_n \exp(jb_n) \end{aligned} \tag{1}$$

where λ is the wavelength, $\overrightarrow{k}\,(\theta,\phi)$ is the unit vector of the observation direction (θ,ϕ) and $\overrightarrow{r_n}$ is the position of the n-th antenna element, $f_n(\theta,\phi)$ is the array factor contributed by the n-th antenna element and b_n is its phase. Note that $\{b_n\}$ is also a function of the observation angle (θ,ϕ), however, to simplify the notation this angle dependence is not shown in the following discussion. Without considering position errors of the antenna elements, the term $\overrightarrow{k}\,(\theta,\phi)\cdot\overrightarrow{r_n}$ is constant at any given direction, then the two phases $\{b_n\}$ and $\{p_n\}$ have the same statistics and can be treated interchangeably.

There are generally two types of excitation errors, namely correlated errors and random errors. Usually, it is the intent of the designer to ensure that the correlated errors are appropriately removed once identified, so that all remained residuals are uncorrelated and random, which are difficult to compensate due to their randomness [24]–[27]. Hence, only random excitation errors are considered in the following discussion. With excitation errors, the real antenna element excitation can

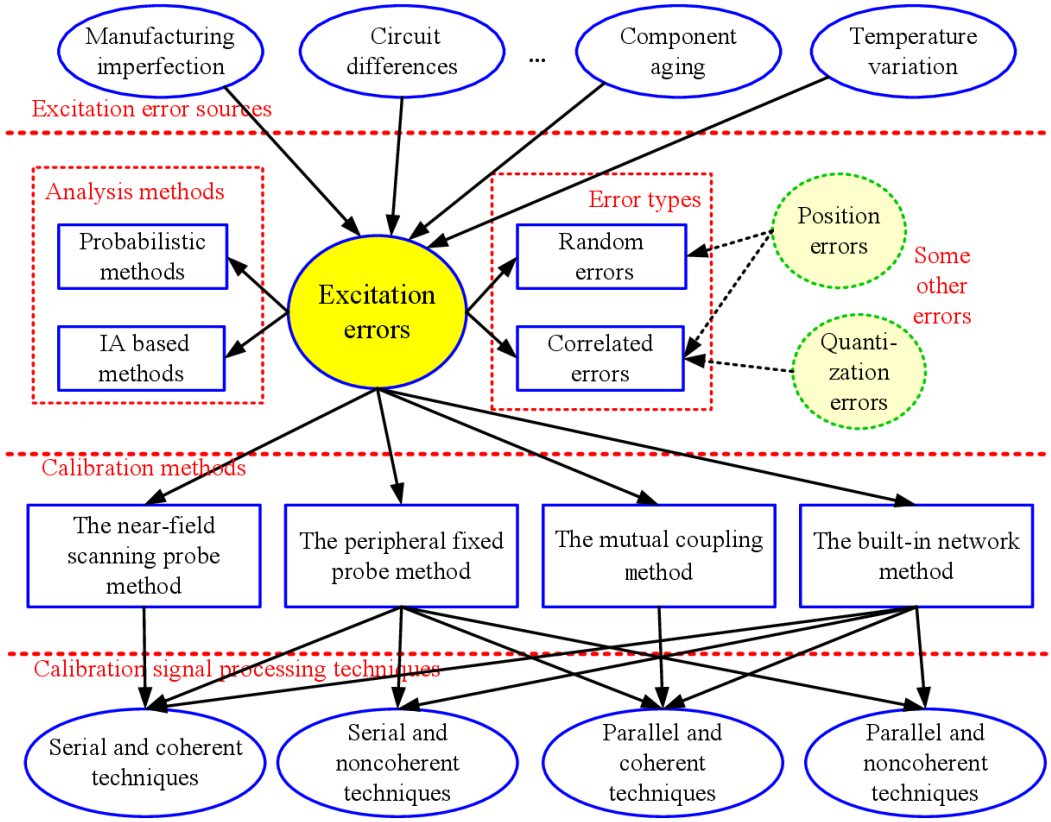

FIGURE 1. The main topics and general flowchart of this paper, including analysis methods, calibration methods, and signal processing techniques of excitation errors for phased array antennas.

be described according to its referenced value,

$$\begin{aligned} a_n^{real} &= a_n(1+\gamma_n) \\ p_n^{real} &= p_n + \delta_n \end{aligned} \tag{2}$$

and without position errors,

$$b_n^{real} = b_n + \delta_n \tag{3}$$

where a_n^{real} and p_n^{real} are the real excitation amplitude and phase of the n-th antenna element, and the random variables γ_n and δ_n represent its relative amplitude error and phase error in percentage and degree, respectively.

Without loss of generality, the variances in the amplitude and phase error are assumed to be identical among antenna elements. According to the central limit theorem, both of these random variables are Gaussian distributed and have zero mean,

$$\begin{aligned} \gamma_n &\approx N(0, \sigma_a^2) \\ \delta_n &\approx N(0, \sigma_p^2) \end{aligned} \tag{4}$$

where σ_a and σ_p are the standard deviations of the excitation amplitude and phase error, respectively.

Figure 2 illustrates an example of a half-wavelength equally spaced ($d = \lambda/2$) 10-element linear antenna array, which is used as the benchmark architecture in the following discussion. The referenced array pattern is Taylor tapered with $SLL^{ref} = -20$ dB and $\bar{n} = 2$, and the corresponding parameters and excitation amplitudes are summarized in Table 1. It has the main lobe with the first nulls at $\theta = \pm 17$ deg, and the highest SLLs (the first sidelobe at $\theta = \pm 19$ deg) are approximately equal to -20 dB as designed. Some Monte Carlo simulations are also presented with $\sigma_a = 0.05$ and $\sigma_p = 5$ deg, whose results show some performance degradation, i.e., higher SLL and broader main beam.

B. THE EXPECTATION OF THE ARRAY PATTERN

The expected array pattern aims to evaluate the average pattern performance and provide approximate formulas for the confidence boundaries. From (1)-(3), the real array pattern $f^{real}(\theta, \phi)$ is rewritten as,

$$f^{real}(\theta, \phi) = \sum_{n=1}^{N} a_n(1+\gamma_n) \exp\left[j(b_n + \delta_n)\right] \tag{5}$$

Generally, the array pattern is a complex value and can be splitted into the real and imaginary parts,

$$\begin{aligned} f_R^{real}(\theta, \phi) &= \sum_{n=1}^{N} a_n(1+\gamma_n) \cos(b_n + \delta_n) \\ f_I^{real}(\theta, \phi) &= \sum_{n=1}^{N} a_n(1+\gamma_n) \sin(b_n + \delta_n) \end{aligned} \tag{6}$$

TABLE 1. The Example of 10-element Taylor Tapered Linear Antenna Array for Probabilistic Analysis.

Quantity	Value
Element number	$N = 10$
Inter-element distance	$d = \lambda/2$
Amplitude Tapering	Taylor tapered with $\mathrm{SLL}^{\mathrm{ref}}$ = -20 dB and $\bar{n} = 2$
Excitation amplitudes	$a_1 = a_{10} = 0.542$ $a_2 = a_9 = 0.629$ $a_3 = a_8 = 0.771$ $a_4 = a_7 = 0.913$ $a_5 = a_6 = 1.000$
Locations of the first nulls	$\theta = \pm 17$ deg
Locations of the first sidelobes	$\theta = \pm 19$ deg
Standard deviation of the amplitude error	$\sigma_a = 0.05$
Standard deviation of the phase error	$\sigma_p = 5$ deg

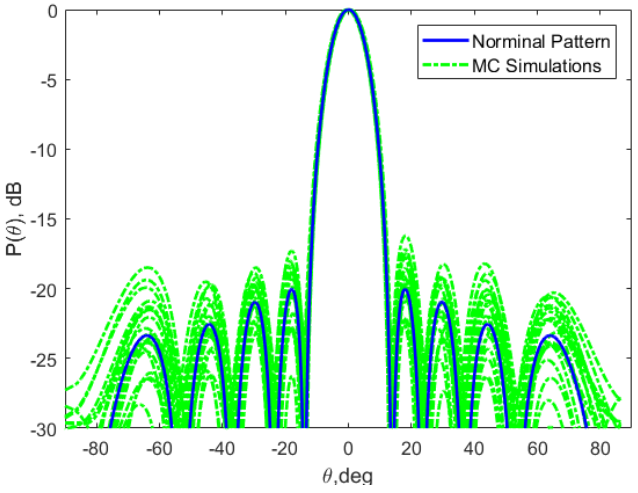

FIGURE 2. The referenced array pattern of the 10-element Taylor tapered linear antenna array, with Monte Carlo simulations are presented with standard deviations of the amplitude error $\sigma_a = 0.05$ and phase error $\sigma_p = 5$ deg.

From the Biggelaar's work [27], the expectations of these two parts, $u_R(\theta, \phi)$ and $u_I(\theta, \phi)$, can be derived as follows,

$$u_R(\theta,\phi) = E\left(f_R^{real}(\theta,\phi)\right) = \exp(-\sigma_p^2/2)\sum_{n=1}^{N} a_n \cos b_n$$

$$u_I(\theta,\phi) = E\left(f_I^{real}(\theta,\phi)\right) = \exp(-\sigma_p^2/2)\sum_{n=1}^{N} a_n \sin b_n \quad (7)$$

And the variances of these two parts, $\sigma_R^2(\theta, \phi)$ and $\sigma_I^2(\theta, \phi)$, have the following expressions,

$$\sigma_R^2(\theta,\phi) = \frac{1}{2}(1+\sigma_a^2)\left[1-\exp(-2\sigma_p^2)\right]\sum_{n=1}^{N} a_n^2 + \left[(1+\sigma_a^2)\exp(-2\sigma_p^2) - \exp(-\sigma_p^2)\right]\sum_{n=1}^{N} a_n^2 \cos^2 b_n$$

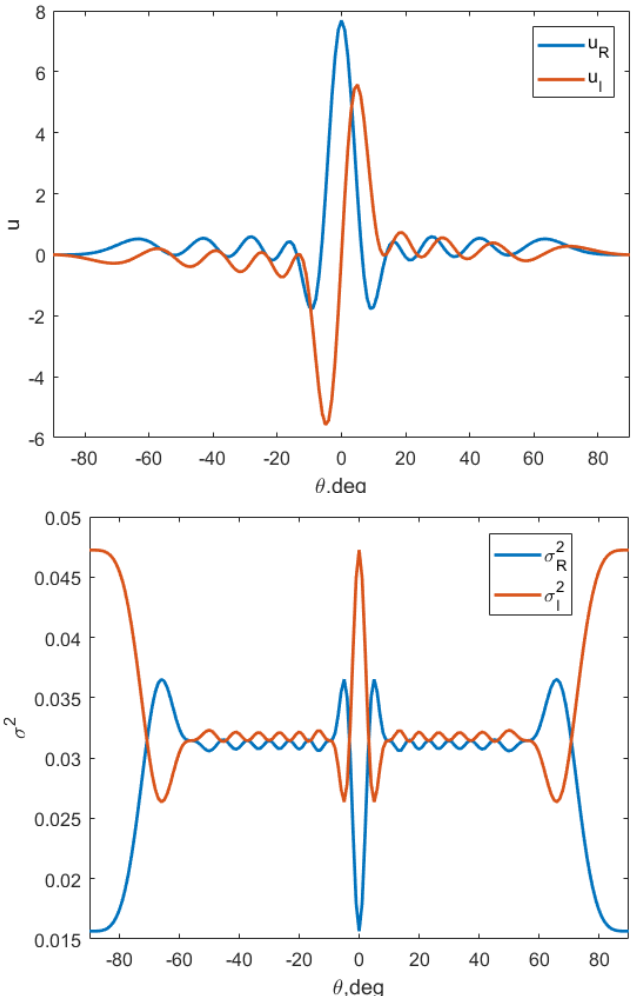

FIGURE 3. The expectations and variances of the real and imaginary parts of the array pattern for the 10-element Taylor tapered linear antenna array.

$$\sigma_I^2(\theta,\phi) = \frac{1}{2}(1+\sigma_a^2)\left[1-\exp(-2\sigma_p^2)\right]\sum_{n=1}^{N} a_n^2 + \left[(1+\sigma_a^2)\exp(-2\sigma_p^2) - \exp(-\sigma_p^2)\right]\sum_{n=1}^{N} a_n^2 \sin^2 b_n \quad (8)$$

Figure 3 illustrates the expectations and variances of the real and imaginary parts of the array pattern. As can be seen, the expectation for the real part is symmetric while the imaginary part is anti-symmetric. Their variances closely follow each other at most of the angles except at the boresight and the grating lobe. This is because the first term of their variances are the same in (8), while the latter term differs in their values especially in these two regions.

From (7) and (8), the expectation of the array power pattern $P(\theta, \phi)$ can be derived as,

$$E\left(P(\theta,\phi)\right) = E\left((f_R^{real}(\theta,\phi))^2\right) + E\left((f_I^{real}(\theta,\phi))^2\right)$$

$$= u_R^2(\theta,\phi) + \sigma_R^2(\theta,\phi) + u_I^2(\theta,\phi) + \sigma_I^2(\theta,\phi)$$
$$= \exp(-\sigma_p^2)\left[\left(\sum_{n=1}^{N} a_n \cos b_n\right)^2 + \left(\sum_{n=1}^{N} a_n \sin b_n\right)^2\right]$$
$$+ (1+\sigma_a^2)\left[1-\exp(-2\sigma_p^2)\right]\sum_{n=1}^{N} a_n^2$$
$$+ \left[(1+\sigma_a^2)\exp(-2\sigma_p^2) - \exp(-\sigma_p^2)\right]\sum_{n=1}^{N} a_n^2$$
$$= \exp(-\sigma_p^2)P^{ref}(\theta,\phi) + \left[1+\sigma_a^2-\exp(-\sigma_p^2)\right]\sum_{n=1}^{N} a_n^2 \quad (9)$$

where $P^{ref}(\theta,\phi)$ is the normal/ideal array power pattern without excitation errors,

$$P^{ref}(\theta,\phi) = |f(\theta,\phi)|^2 = \left|\sum_{n=1}^{N} a_n \exp(jb_n)\right|^2$$
$$= \left[\left(\sum_{n=1}^{N} a_n \cos b_n\right)^2 + \left(\sum_{n=1}^{N} a_n \sin b_n\right)^2\right] \quad (10)$$

This expression in (9) shows that the effect of random excitation errors produces the real array power pattern consisting of the ideal pattern reduced by a factor that accounts for phase error, plus another term that is a constant with no angular dependence [13]. It is convenient to normalize the latter term to the peak of the resulting pattern, and the normalized sidelobe level is given by,

$$SLL = \frac{\left[1+\sigma_a^2-\exp(-\sigma_p^2)\right]\sum_{n=1}^{N} a_n^2}{\exp(-\sigma_p^2)(\sum_{n=1}^{N} a_n)^2}$$
$$= \left[\left(1+\sigma_a^2\right)\exp(\sigma_p^2) - 1\right]\sum_{n=1}^{N} a_n^2 \Big/ (\sum_{n=1}^{N} a_n)^2$$
$$\approx \left[\left(1+\sigma_a^2\right)\left(1+\sigma_p^2\right) - 1\right]\sum_{n=1}^{N} a_n^2 \Big/ (\sum_{n=1}^{N} a_n)^2$$
$$\approx \left(\sigma_a^2+\sigma_p^2\right)\Big/ N\eta_A \quad (11)$$

where η_A is known as the array taper efficiency [28],

$$\eta_A = (\sum_{n=1}^{N} a_n)^2 \Big/ N\sum_{n=1}^{N} a_n^2 \quad (12)$$

The symmetrical form of the amplitude and phase errors in (11) suggests the convenience of converting them from one to the other. This helps in the trade-off to determine how much of the error variance to allot between the two [25]. Figure 4 presents several curves of average sidelobe level due to the phase and amplitude errors for the linear array as presented in Table 1. Due to their interchangeability, each sidelobe level curve is like an arc.

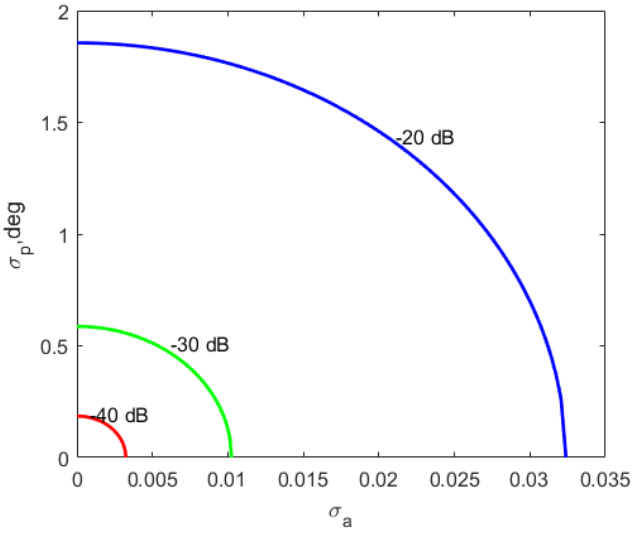

FIGURE 4. Array average sidelobe level due to phase and amplitude errors for the 10-element Taylor tapered linear antenna array.

C. THE PDF OF THE ARRAY PATTERN

As can been seen in Fig. 3, for most regions except at the boresight, grating lobe, and other selective regions, it's reasonable to assume that the real and imaginary parts of the array factor have identical mean value and share the same variance. Hence, as sum of these two Gaussian distributed variances, the array pattern at these regions follows Rician distribution with the PDF defined as,

$$prob(r(\theta,\phi)) = \frac{r(\theta,\phi)}{\sigma_r^2(\theta,\phi)} \exp\left(-\frac{r^2(\theta,\phi)+u_r^2(\theta,\phi)}{\sigma_r^2(\theta,\phi)}\right) \cdot I_0\left(\frac{r u_r(\theta,\phi)}{\sigma_r^2(\theta,\phi)}\right) \quad (13)$$

where $I_0()$ is the modified Bessel function of the first kind with order zero, and

$$u_r(\theta,\phi) = \sqrt{u_R^2(\theta,\phi) + u_I^2(\theta,\phi)}$$
$$\sigma_r^2(\theta,\phi) = \frac{1}{2}\left(\sigma_R^2(\theta,\phi) + \sigma_I^2(\theta,\phi)\right) \quad (14)$$

Generally, the same variance assumption is good enough for most analyses. However, it has been pointed out that this assumption is not mandatory and a Beckman distribution can be derived [27]. For other special regions that have unidentical variances for the real and imaginary parts, such as the boresight ($u_I = 0$) and null locations ($u_R = u_I = 0$), detailed mathematical derivation can be found in Bhattacharyya's excellent book [29].

III. IA BASED METHODS FOR ARRAY PATTERN BOUND ESTIMATION

For practical antenna array engineering, it's of great interest to evaluate the worst performance of the array pattern along with statistical characteristics. Recently, the IA technique was introduced by P. Rocca *et al.* [30],

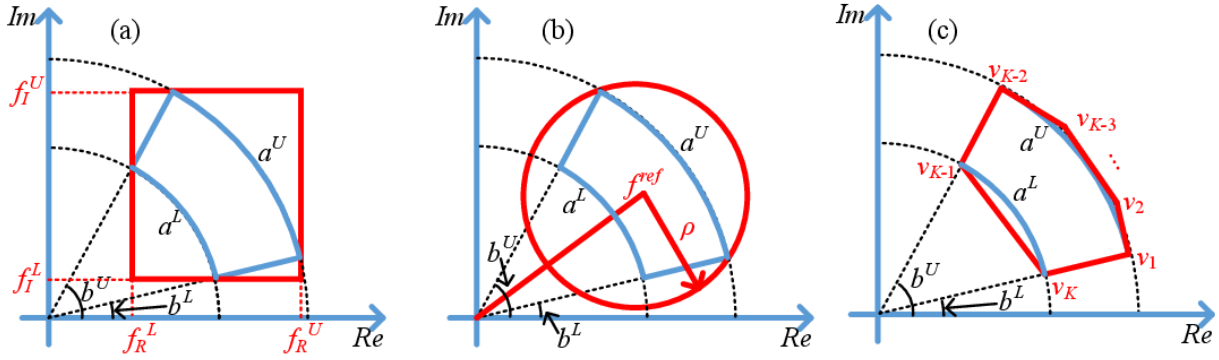

FIGURE 5. Illustration of three IA based methods, (a) the Cartesian IA method, (b) the Circular IA method, and (c) the Polygonal IA method. The boundary of each element is defined by the amplitude interval $[a^L, a^U]$ and phase interval $[\theta^L, \theta^U]$. $[a_R^L, a_R^U]$ and $[a_I^L, a_I^U]$ represent the interval of the real and imaginary parts in the Cartesian IA method, respectively. The boundary for Circular IA method is represented with $< f, \rho >$ denoting the center f and the radius ρ, while the Polygonal IA method uses a convex polygon with K vertexes $\{v_n\}$.

Anselmi *et al.* [31]–[33], [35], Massa *et al.* [34], and Tenuti *et al.* [36] to evaluate the effects of excitation errors and the corresponding upper and lower bounds of the array patterns. Thanks to the intrinsic of IA to deal with uncertainties, it's very efficient to determine the bounds of array patterns in a robust and reliable way. It needs no detailed information unless the knowledge of the intervals about the excitation errors, which are the only terms involved in the IA based mathematical operations. As shown in Figure 5, according to the geometry of the excitation error representation, three IA based methods have been proposed, i.e., the Cartesian IA method, the Circular IA method, and the Polygonal IA method.

A. THE CARTESIAN IA METHOD

As shown in Fig. 5(a), a specified excitation error has a fan-like geometry defined by the boundaries of amplitude interval $[a^L, a^U]$ and phase interval $[b^L, b^U]$. Please keep in mind that b^L and b^U are also dependent on the observation direction (θ, ϕ). For the Cartesian IA method, the error geometry is expanded into the rectangular form for convenience [30], [31]. Again, the complex array pattern of (1) is rewritten with the real part $f_R(\theta, \phi)$ and the imaginary part $f_I(\theta, \phi)$,

$$\begin{aligned} f(\theta, \phi) &= f_R(\theta, \phi) + j \cdot f_I(\theta, \phi) \\ &= \sum_{n=1}^{N} a_n \cos b_n + j \cdot \sum_{n=1}^{N} a_n \sin b_n \end{aligned} \tag{15}$$

The array power pattern $P(\theta, \phi)$ can be obtained by first squiring these two parts then adding them together,

$$\begin{aligned} P(\theta, \phi) &= P_R(\theta, \phi) + P_I(\theta, \phi) \\ &= |f_R(\theta, \phi)|^2 + |f_I(\theta, \phi)|^2 \end{aligned} \tag{16}$$

Since $a_n > 0$, the bound of the real part of the array pattern $[f_R^L(\theta, \phi), f_R^U(\theta, \phi)]$ can be derived as

$$f_R^L(\theta, \phi) = \sum_{n=1}^{N} a_n^L (\cos b_n)^L$$

$$f_R^U(\theta, \phi) = \sum_{n=1}^{N} a_n^U (\cos b_n)^U \tag{17}$$

where

$$(\cos b)^L = \begin{cases} -1 & if\ (2k+1)\pi \in [b^L, b^U] \\ \min\left\{\cos(b^L), \cos(b^U)\right\} & otherwise \end{cases} \tag{18}$$

$$(\cos b)^U = \begin{cases} 1 & if\ 2k\pi \in [b^L, b^U] \\ \max\left\{\cos(b^L), \cos(b^U)\right\} & otherwise \end{cases} \tag{19}$$

A similar expression can be obtained for the imaginary part, and the interval of the array power pattern is as,

$$\begin{aligned} P^L(\theta, \phi) &= P_R^L(\theta, \phi) + P_I^L(\theta, \phi) \\ P^U(\theta, \phi) &= P_R^U(\theta, \phi) + P_I^U(\theta, \phi) \end{aligned} \tag{20}$$

It should be mentioned that, due to the intrinsic of the complex notation, the real and imaginary parts of the array pattern in (15) are dependent and highly correlated to each other. If an interval variable occurs several times in the expression, and each occurrence is taken independently, then this so-called dependency problem will cause expansion of the resulting intervals. In the above derivation, the array excitation error occurs in both the real and imaginary parts, this will cause an unwanted overestimation when adding them together [37], [38].

B. THE CIRCULAR IA METHOD

For the circular IA method, as shown in Fig. 5(b), the geometry of the excitation error is represented into the circular form. It's denoted as $< f(\theta, \phi), \rho(\theta, \phi) >$, where $f(\theta, \phi)$ is the center and $\rho(\theta, \phi)$ is the radius covering all possible excitation error values [35]. The advantage of the circular IA method is the simplicity of IA calculation, the radius of the array pattern is the sum of the radius of the interval of each

element, respectively,

$$\rho(\theta,\phi)=\sum_{n=1}^{N}\rho_n(\theta,\phi) \tag{21}$$

where $\rho_n(\theta,\phi)$ is the radius covering the excitation error of the n-th element,

$$\begin{aligned}\rho_n(\theta,\phi)=\max\{&\left|a_n\exp(jb_n)-a_n^L\exp(jb_n^L)\right|,\\&\left|a_n\exp(jb_n)-a_n^L\exp(jb_n^U)\right|,\\&\left|a_n\exp(jb_n)-a_n^U\exp(jb_n^L)\right|,\\&\left|a_n\exp(jb_n)-a_n^U\exp(jb_n^U)\right|\}\end{aligned} \tag{22}$$

The bounds of the array power pattern are obtained by first calculating the bounds of the array pattern and then squaring it,

$$\begin{aligned}P^U(\theta,\phi)&=(|f(\theta,\phi)|+\rho(\theta,\phi))^2\\P^L(\theta,\phi)&=\begin{cases}(|f(\theta,\phi)|-\rho(\theta,\phi))^2\\\quad if\quad |f(\theta,\phi)|>\rho(\theta,\phi)\\0\quad otherwise\end{cases}\end{aligned} \tag{23}$$

In this way, the excitation of the antenna element as an interval variable appears only once in (21). However, the radius is enlarged due to the expression of the circular IA form.

C. THE POLYGONAL IA METHOD

As shown in Fig. 5(c), a more compact geometry is to expand the excitation error region as a convex polygon. The outer arc of the possible region is surrounded by several tangent lines, while the inner arc is surrounded by a line between the two vertices. In such a case, the computation procedure of the sum of two convex polygons is known as the Minkowski sum. Let V and W be two convex polygons representing possible regions of the excitation errors of two antenna elements with K vertices $\{v_1,\ldots,v_K\}$ and M vertices $\{w_1,\ldots,w_M\}$, respectively. Their Minkowski sum can be computed as follows [39],

Step 1: initial $k=1, m=1$;

Step 2: add v_k+w_m as the vertex of the sum.

Step 3: if angle$(v_kv_{k+1})\le$ angle(w_mw_{m+1}), then $k=k+1$;

else if angle$(v_kv_{k+1})\ge$ angle(w_mw_{m+1}), then $m=m+1$;

else $k=k+1, m=m+1$.

Step 4: repeat step 2 and step 3 until $k=K+1$ and $m=M+1$.

The above procedure runs in linear time because at each execution of the repeat loop either k or m is incremented. Moreover, the Minkowski sum is also a convex polygon with at most $K+M$ edges [39]. Hence, By sequentially adding each element with N-1 times of Minkowski sum calculation, the interval of the array pattern can be obtained with improved bounds thus more reliable results. An extensive comparison of these three IA based methods with representative numerical results can be found in [32]. Generally speaking, the Polygonal IA method performs the best for most scenarios, while the Circular IA method performs the worst. An analytic method is also proposed to analyze and further dig the information from the shape of the convex polygon of the array pattern, and map it into the probability distribution of the bound interval [40].

IV. CALIBRATION METHODS

The objective of phased array antenna calibration is to sample each antenna element in the array, and compare the obtained results to identify the differences among the elements. Phased array calibration for both transmit and receive are similar, the primary differences lie in the test-signal distribution at the input and the combination at the output. For receive calibration, a calibration source and/or a distribution network is required to inject the test signal into the input of each element, the array beamformer can be used as a test signal combiner. For transmit calibration, it requires a calibration source signal into each element and additional equipment or beam combiner for combined signal monitoring. Only receive calibration is presented here to keep the discussion focused, the extension for transmit calibration is straightforward. The calibration methods vary from different systems and applications, either suitable for factory test or for in-field test. According to Seker's work [41], these calibration methods can be generally divided into four main categories, i.e., the near-field scanning probe method, the peripheral fixed probe method, the mutual coupling method, and the built-in network method. The advantages and challenges of these calibration methods are shortly summarized in Table 2 and presented in the following subsections.

A. THE NEAR-FIELD SCANNING PROBE METHOD

The traditional near-field scanning probe method, also known as "park and probe", is one of the most widely used methods in the industry for phased array antenna calibration [42]–[46]. It's considered to be very reliable and accurate with element-level pattern accuracy as high as 0.1 dB and 0.1 deg, respectively [42]. The procedure is straightforward, the tested element is excited to its default state, a robotic manipulator places a near-field scanning probe antenna at the boresight of the tested element, to directly measure the relative phase and amplitude by Vector Network Analyzer (VNA). Then it moves to test the next element under the same testing condition, and repeats this procedure until all elements of the antenna array are tested. As depicted in Fig. 6(a), supposing g_p^t is the transmit gain of the calibration probe, C_{pn} is the coupling coefficient between the probe antenna and the n-th antenna element under test, and g_n^r is the receive gain of the n-th element to be calibrated. Then the signal received by the n-th antenna element R_{pn} can be formulated as,

$$R_{pn}=g_p^tC_{pn}g_n^r \tag{24}$$

TABLE 2. The advantages and Challenges of Phased Array Calibration Methods.

Method	Advantages	Challenges
The near-field scanning probe method	Reliable and accurate.	Requiring a precise automated mechanical system. Time-consuming. Only suitable for in-factory test.
The peripheral fixed probe method	Widely used in-field test. Calibration can be done in parallel. Calibration can be done in noncoherent.	Requiring additional hardware. Involving complicated signal processing.
The mutual coupling method	No external equipment required. Calibration can be done in parallel.	Would encounter unwanted edge effect.
The built-in network method	High accuracy and efficiency. Calibration can be done in parallel. Calibration can be done in noncoherent.	Requiring dedicated coupling network.

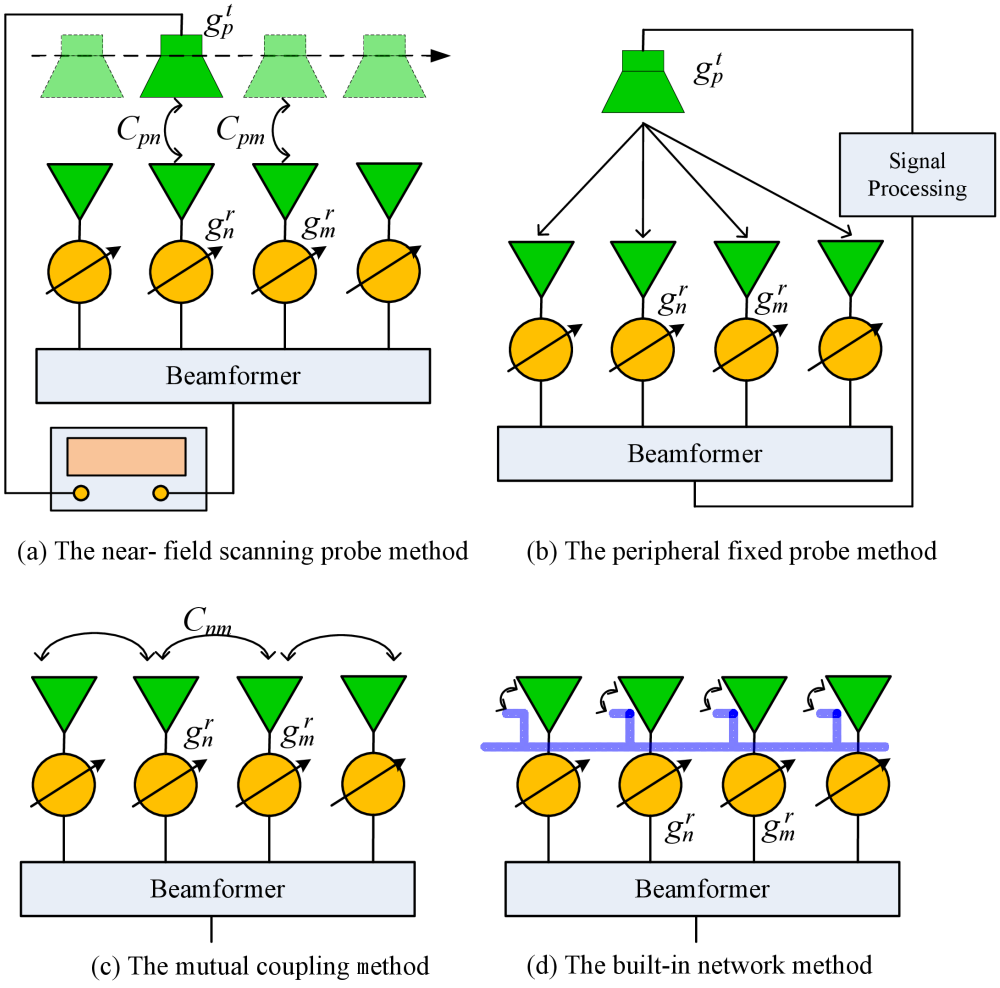

(a) The near- field scanning probe method (b) The peripheral fixed probe method

(c) The mutual coupling method (d) The built-in network method

FIGURE 6. Simplified diagram of the phased array calibration methods.

Analogously, the signal received by the m-th antenna element R_{pm} can be formulated as,

$$R_{pm} = g_p^t C_{pm} g_m^r \tag{25}$$

Since the technique scans and tests all the antenna elements under the same conditions, it assumes that the coupling coefficient between the probe and the tested element is the same for all array elements, i.e., $C_{pn} = C_{pm}$. Hence, the relative excitation error between these two elements can be obtained as,

$$\frac{g_n^r}{g_m^r} = \frac{R_{pn}}{R_{pm}} \tag{26}$$

Usually, probe position error will result in some of the measurement error in near-field measurement [47]. However, for phased array near-field scanning probe calibration, it is not necessary to keep the probe antenna precisely at the boresight

of each antenna element under test. It is sufficient to just keep the relative position and angle between the probe antenna and the tested element unchanged. In that case, even if the probe is somewhat offset from its desired position for every antenna element, the amount of offsets and therefore couplings will be still the same for all tested antenna elements, making this technique still useful.

The near-field scanning probe method usually requires a precise automated mechanical system including elements such as the axes controllers, actuators, motors for accurate probe movement. This makes the setup suitable to work only in the near-field environment, but too complicated to arrange it in the field test. Moreover, due to the mechanical movement of the probe antenna, the measurement process is very time-consuming, especially for large-scale phased array antennas. For example, for the THAAD (Theater High Altitude Area Defense) radar, each of the 25,344 T/R modules had to be near-field scanned individually, result in a very long and even unacceptable test time [48], [49]. Therefore, the near-field scanning probe method is most suitable for initial factory test rather than periodic in-field calibration.

B. THE PERIPHERAL FIXED PROBE METHOD

In some large phased array antennas, unlike the near-field scanning method with a moveable probe antenna, one or several fixed probe antennas are placed at the periphery of the array [50]–[54], or moving platform such as a balloon or unmanned aerial vehicle (UAV) [55], [56]. In [57], calibration is made by external fixed probe antennas at certain locations near the array. A circle around the array center is chosen for symmetry reasons. It's proposed that one probe antenna is integrated at the side for a spaceborne phased array calibration [58]. High calibration accuracy can be achieved for actual satellite systems because this allows easy realization with high signal-to-noise ratio (SNR). The Space Fence, used to detect, track, and catalog small objects in Space Situational Awareness for the U.S. Air Force Space Surveillance Network, both the transmit and receive arrays are calibrated with horn antennas mounted on calibration towers in the near-field [59].

If the fixed probe is at the far-field of the array under test, then the effects of each antenna element can be viewed as the same. Otherwise, the coupling between the probe and each antenna element is going to be different. In this case, the peripheral fixed probe method can be applied only if the coupling amounts were previously measured or calibrated and moved out. This can be done by using a near-field scanning probe in factory test, then compared with the results from peripheral fixed probes made in-field to calculate the couplings. For example, the SAMPSON Multi-Function Radar has four fixed open waveguide auxiliary radiators used for calibration [60]. The signal received from an individual active channel is compared with a stored reference level obtained during the factory test of the phased array antenna. In this way, a replacement module or one whose characteristics have simply drifted with time may be reset to the original RF performance, thus restoring the original factory-fresh condition of the antenna. With the peripheral fixed probe method, some advanced signal processing techniques can be adopted to reduce the complexity of measurement hardware requirements, which is presented in detail in Section 5.

C. THE MUTUAL COUPLING METHOD

The mutual coupling method was first proposed by Aumann *et al.* [61] on a linear antenna array, based on the idea that the inherent mutual coupling among the array elements can be used by transmitting from an element and receiving from another. The measured signals between all pairs of elements in the array allow a complete characterization of the relative amplitude and phase of each element in the array. Compared to the near-field scanning probe method and the peripheral fixed probe method, this method utilizes the inherent property of mutual coupling and requires no external hardware resources, resulting in a much faster calibration process and more suitable for in-field calibration [62]–[68].

The mutual coupling method was extended to two-dimensional (2D) antenna array and became more practically useful [63]. The detail of the mutual coupling method depends on the specific array geometry. Taking the most common rectangular array as an example, as shown in Fig. 7, there are four elements under test and two parameters need to be calibrated for each element. Let g_m^t denotes the transmit gain of the m-th element and g_n^r denotes the receive gain of the n-th element to be calibrated. A mutual coupling measurement consisting of a signal transmitted from the m-th element and received by the n-th element. When the #2 and #3 elements as receive and the #1 and #4 elements as transmit, two pairs of mutual coupling measurements are formulated as,

$$\begin{aligned} R_{12} &= g_1^t C_{12} g_2^r, \quad R_{13} = g_1^t C_{13} g_3^r \\ R_{42} &= g_4^t C_{42} g_2^r, \quad R_{43} = g_4^t C_{43} g_3^r \end{aligned} \tag{27}$$

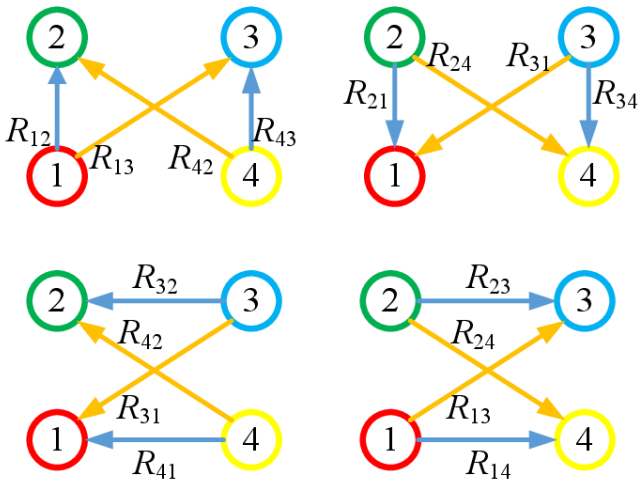

FIGURE 7. Coupling schemes for rectangular phased array calibration by performing the mutual coupling method [41], [70].

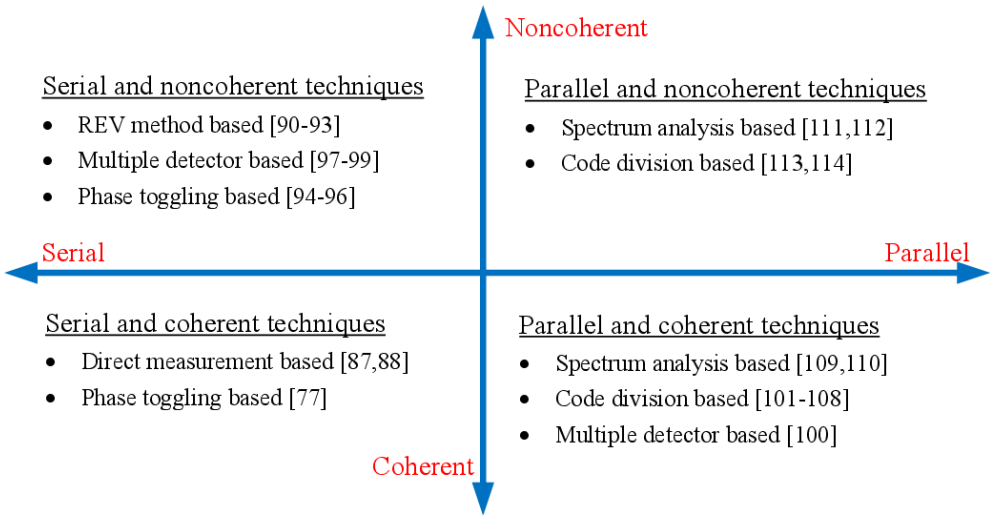

FIGURE 8. Signal processing techniques for phased array calibration.

From these four measurements, these elements can be calibrated relative to each other as,

$$\frac{g_2^r}{g_3^r} = \left(\frac{R_{12}R_{42}}{R_{13}R_{43}}\right)^{1/2}, \quad \frac{g_1^t}{g_4^t} = \left(\frac{R_{12}R_{13}}{R_{42}R_{43}}\right)^{1/2} \tag{28}$$

From the other three topographies with six more pairs of measurements, the relative transmit and receive gains of all four elements can be solved. Moreover, a mathematical framework by the least square method is proposed that using measurement results as many as possible [69].

There is also something to be mentioned for the mutual coupling method. It relies on the assumption that coupling between an antenna element and its neighbors are the same for all elements in the array. Nonetheless, it was revealed by using a prototype system, it does not hold for small arrays due to unwanted edge effects [70], [71]. A before/after approach is introduced to avoid errors introduced by edge effects, the ratio between the after and before status will quantify the changes suffered by the elements.

D. THE BUILT-IN NETWORK METHOD

It's very common to use a built-in network connected to each antenna element for periodic in-field calibration of integrated phased array antennas, especially for Si-based RF and mmWave-band integrated phased array [22], [72]–[82]. As shown in Fig. 6(d), this technique employs microstrip transmission line as test signal injector or weak signal coupler embedded under the element for calibration, with the coupling ratio between the transmission line and the radiating element usually several tens of dB. These calibration lines sample the signals received or transmitted by the antenna elements. The measured signals are then used to calculate the amplitude and phase differences among the elements. An early example of built-in performance monitoring system was developed and tested in [77]. Test distribution networks can also be integrated with advanced signal processing techniques on-chip as described in Section 5.

To successfully calibrate a phased array using this method, phase shifts and amplitude losses caused by the transmission lines and the couplers that connect them should be equal or already known. A high-quality, embedded calibration network near the array face could source or receive nearly identical signal levels at each element. If the transmission lines are built using the same material and have the same radius and length, their effects would be very similar. For example, the ELTA/IAI Systems used microstrip line couplers near parallel plate waveguide radiators to individually probe T/R modules through the analog beamformers to supplement initial near-field calibration. The TerraSAR-X imaging satellite was one of the first SAR systems using embedded coupling to supplement the initial calibration once it is launched into space [83], [84]. For the S-band digital array testbed at Lincoln Laboratories, a coupler was used for injecting in front of the LNAs for receive-only calibration monitoring [85]. In [86], a coupled line network that is weakly coupled to the antenna array is designed to provide a calibration signal path without adding any switch after the antenna port.

V. SIGNAL PROCESSING TECHNIQUES FOR PHASED ARRAY CALIBRATION

For the peripheral fixed probe method and the built-in network method for phased array calibration, it's very convenient to apply advanced signal processing techniques to save hardware or time requirements. As shown in Fig. 8, these techniques can be distinguished as serial or parallel by the number of elements to be calibrated each time. In serial calibration techniques, the antenna elements are characterized one by one, and the characterizations of different array elements are independent. Some techniques save time by handling several calibrations simultaneously, thus can be viewed

as more efficient. These techniques can also be distinguished as coherent or noncoherent by the measurement requirements between the calibration source and the element under calibration. For coherent measurement, it's required that the calibration source and sink must be coherent to obtain the complex value containing both amplitude and phase information. On the contrary, noncoherent measurement requires no such synchronization, which can be done by amplitude or power only measurements. All these four kinds of techniques can be conducted with both the peripheral fixed probe method and the built-in network method, only slight differences in the measurement setup are required depending on practical applications.

A. SERIAL AND COHERENT TECHNIQUES

The serial and coherent techniques simply calibrate each element serially and require a coherent measurement to gather the element excitation information. The near-field scanning probe method can also be conducted as one of such kind of techniques. For some smart antenna applications [87] and mobile satellite communication applications [88], [89], these simple and direct calibration techniques are very common, especially with the element-level digital phased array. One of the main advantages of digital beamforming over every element is the ease that amplitude and phase errors among elements can be calculated in the digital domain.

There are also some measurement setups involving phase toggling. In [77], the phase of the element under calibration is switched between two states of 0 and π, while the other elements stay unchanged. By comparing the combined array signal of these two measurements, the element excitation can be easily determined, while the other stationary element outputs can be canceled out.

B. SERIAL AND NONCOHERENT TECHNIQUES

Compared to coherent measurement methods, noncoherent techniques which involve amplitude or power only measurements are considered to be more convenient. In such a case, coherent measurements are no longer required with precise synchronization between the calibration source and the element under calibration. However, this is usually done with some additional costs. e.g., more power detectors or more times of measurements. The rotating element electric field vector (REV) method is the most well-known power only measurement method with only one power detector. It measures the amplitude of the array combined signal by shifting the element phase from 0 to 2π continuously [90]–[93]. The element excitation can be determined from statistics of three parameters, the maximum and minimum power of the array signal, and the element rotation phase to maximum power.

In [94], it was pointed out that measurement results at four orthogonal phase shifts are sufficient enough to obtain a maximum likelihood estimation for each array element. An even simpler expression was further derived in [95] that requires only two phase shifts of $\pi/2$ and π to yield the element complex excitation information. Another novel power only measurement method is derived to calibrate the element excitation [96]. For each array element, two power measurements are used to determine the element complex excitation, one by shifting the element's phase of $\pi/2$ and the other by turning the element under test off. From the mathematical point of view, it's required at least two amplitude (power) measurements to determine the complex excitation of one array element.

In [97], [98], multiple noncoherent power detectors are distributed across the array for amplitude and phase extraction. Power detectors can also be placed between adjacent elements, allowing the measurement of relative phase in addition to amplitude [99].

C. PARALLEL AND COHERENT TECHNIQUES

Compared to serial techniques, parallel techniques that simultaneously calibrate a number of array elements are more efficient, which is especially suitable for large phased arrays with small calibration time slots. Some parallel techniques measure the array combined signals with several measurement probes at multiple positions [100]. However, this requires some hardware burden. A more popular alternative technique allows simultaneously measuring excitations of multiple elements relying on code modulation [101]–[105]. A method that controls the element phases based on time multiplexed orthogonal codes was proposed in [101], thus the individual element excitation can be derived from the combined array signal. The pseudo-random (PN) code for phased array calibration has been successfully verified in a space born environment by TerraSAR-X [106]. In addition, a similar technique with Walsh codes was used for Sentinel-1 [107]. A recursive matrix-forming method for Hadamard matrix construction is presented in [108] for phased array calibration.

Besides these aforementioned methods, the spectrum analysis technique can also be adopted for phased array parallel calibration. In [109], [110], a multi-element phase toggling method with Fast Fourier Transform (FFT) based spectrum analysis is proposed for parallel calibration. Each element under calibration is toggled with a particular odd time of fundamental step frequency. By applying FFT analysis of the combined complex signal, both the amplitude and phase of each element can be found in the corresponding spectrum.

D. PARALLEL AND NONCOHERENT TECHNIQUES

The parallel and noncoherent techniques, with multi-element element calibration each time and no coherent measurement required, should be the most preferred technique at the expense of more complex signal processing. In [111], the phases of multiple antenna elements are successively shifted with the specified phase intervals. The measured array power variation is expanded into Fourier series and the terms are rearranged to put them into the form of the conventional REV method. In [112], another spectrum analysis based method is proposed by periodically modulating the element phase sequentially. The phase of the antenna element is

shifted to π on one time slot while staying unchanged for the other time slots. By applying FFT analysis of the combined array signal, the element complex excitation is obtained from the corresponding modulation frequency harmonics.

In [113], [114], a novel calibration technique that employs code-modulated interferometry is proposed for parallel measurements. Moreover, it requires only a simple power squaring detector without the need for a coherent receiver. First, the common test signal in the form of a single-frequency tone injected into each element, both the in- and quadrature-phase components of each element are encoding, then combined and squared using an on-chip power detector. Benefiting those orthogonal code products (OCPs) where the product of any two codes is another unique code, the squaring operation downconverts the combined signal to baseband and creates an interference pattern between all of the individual elemental responses. This pattern contains complex cross-correlations that are each modulated according to the OCP. Using each OCP, the correlation of interest can be demodulated, and then the full set of correlations can be used to extract amplitude and phase information for all elements.

VI. SOME OTHER COMMON ERRORS

Although the excitation errors are analyzed in this paper, the real phased array antenna will suffer some other errors in practice. Here two other common errors of phased array antenna, position errors and quantization errors, are shortly discussed to inspire the readers' broader envision for phased array antenna calibration.

A. POSITION ERRORS

As described in Section II-A, the position errors of array elements will also influence the performance of the array. A large number of studies have been focusing on the position tolerance of antenna elements [115]–[118]. A coupled structural-electromagnetic model is developed to evaluate the effects of random position errors on the performance of phased antenna arrays [116], [117]. The relationship between the position tolerance of the antenna element and the gain loss of the array is derived in [118]. A conical scheme for representing element position errors is proposed in [119], which considers both the relevance and the randomness of the position errors of adjacent planar array elements. The IA based method is also applied to evaluate the effects of element position errors on the statistic performance [120].

B. QUANTIZATION ERRORS

With the advance of modern RF technologies, digital amplitude attenuators and digital phase shifters are nowadays extensively used than analog ones. Thus, the optimized continuous amplitude and phase must be rounded off to the closest quantized value for implementation in practice [121], [122]. Since the errors of these approximate phase and amplitude are highly correlated rather than random, this often yields large grating lobes and degrade the array sidelobe performance. Detailed derivations about array performance degradation and grating lobe levels due to quantization can be found in [13]. To reduce the grating lobe, it is common engineering practice to randomize the amplitude and phase quantization errors thus break up the periodicity. A detailed comparison of several methods can be found in [123] that are used to reduce the peak sidelobe level.

VII. OPEN RESEARCH DIRECTIONS

Currently, phased array calibration is still one of the hottest research topics for phased array technology. Many aspects are expected to be improved with higher efficiency and better performance. Two open research directions, from the authors' personal point of view, are presented here to encourage future researches about phased array calibration.

A. WIDEBAND PHASED ARRAY CALIBRATION

The higher data rate requirements for future wireless communications have significantly driven the need for wideband phased array antennas. Future phased array antennas must address very wideband signals as well as nonlinear behaviors, adaptivity, and reconfigurability. Hence, array calibration techniques must have to be developed to meet such challenges as spurious signals and pulse dispersion for wideband antenna arrays [124], [125]. The phase-shift approximation used in the narrowband beamformer implementation is not valid for processing wideband signals. True time delay (TTD) units rather than phase-shifters are required for wideband beamforming. Several methods have been proposed for wideband phased array calibration. For very long baseline interferometry (VLBI) in radio astronomy, comb tones with a step frequency of several MHz are used to provide wideband and high-stability calibration. The comb tones are injected into the receiver front end to calibrate the phase delay of receive channel over wide band [126]–[128]. Another mainstream idea is to compensate for the channel imbalances corresponding to the channel response. In [129], a digital wideband phased array working on 1-8 GHz is first characterized using impulse response measurement. A chirp signal is injected as the probing signal to measure all 16 channels simultaneously. Based on the spectrum-modified time reversal technique, the impulse response is compensated and both phase and amplitude are realigned for all elements. In the future, more efficient calibration methods are expected to reduce the complexity of measurement setup and calibration signal processing.

B. MACHINE LEARNING BASED CALIBRATION TECHNIQUES

The rise and proliferation of artificial intelligence (AI) has found numerous applications including natural language processing, remote sensing, image recognition, and fraud detection. Machine learning (ML) approaches are scientific disciplines that build a mathematical model based on training data, to enable AI by improving an outcome through the experience without being explicitly programmed. Some popular ML techniques are radial basis functions (RBFs),

support vector machines(SVMs), artificial neural networks (ANN), and deep neural networks (DNNs), just to name a few [130], [131]. Recently, it has also been gaining increasing popularity in the antenna and propagation community to solve complex electromagnetic problems [132]–[134]. For phased array calibration, a graph coloring theory based method is proposed in [135], which transforms the calibration problem into a coloring problem that aims at minimizing the number of used colors. In [136], the number of calibration measurements is minimized by using a compressed sensing (CS) approach. Sparsity is introduced into the combined signals by assigning binary delay vectors, which allows to recovery excitation of individual array elements in a computationally effective way. In [137], the ANN approach is applied to calibrate both transmit and receive channels for phased array antenna, which allows simple hardware implementation and requires little computational power. ML techniques are undoubtedly great analysis tools, particularly for problems with large and complex data sets. As ML techniques grow in sophistication and are still in boosting, more powerful ML based calibration techniques and practical applications are expected for phased array calibration and status monitoring.

VIII. CONCLUSION

Phased array antennas require precise excitation of each antenna element by various synthesis techniques to obtain desired array pattern features. However, because of mechanical manufacturing imperfections, component aging, temperature variation, and circuit differences, the realistic antenna element excitation inevitably differs from their expected values in practice. These errors would cause array pattern distortion, gain degradation, worse SLL, and null drifts. This paper aims to present a tutorial-like review of impact analysis and state-of-the-art calibration methods to overcome excitation errors for phased array antenna. The probabilistic methods provide simple closed-form expressions of the features of the array pattern by exploiting the central limit theorem. The IA based methods introduce intervals to represent the element excitation errors and predict the array performance with its upper and lower bounds. Thanks to the inclusion property of IA to deal with uncertainties, the determined bounds of antenna array pattern are finite and inclusive thus reliable.

To meet the requirements and maintain acceptable performance, phased array antennas must be carefully calibrated to compensate the errors as low as possible. These calibration methods vary from different systems and applications, either suitable for factory test or for in-field test. The near-field scanning probe method that employs a robotic scanner is well-known and widely used as the standard for factory test. The peripheral fixed probe method requires external probes with calibration signal processing. In contrast, the mutual coupling method takes advantage of the inherent property of mutual coupling among elements of the array, and uses it to avoid the employment of external equipment. Some dedicated coupling network that using transmission lines connected to each antenna element for the periodic in-field calibration of integrated phased array antenna, especially for RF and mmWave-band integrated phased array. It's very convenient to apply advanced signal processing techniques to save hardware or time requirements. These techniques can be distinguished as serial or parallel by the number of elements to be calibrated each time, or distinguished as coherent or noncoherent by the measurement requirements between the calibration source and the element under calibration.

REFERENCES

[1] R. L. Haupt and Y. Rahmat-Samii, "Antenna array developments: A perspective on the past, present and future," *IEEE Antennas Propag. Mag.*, vol. 57, no. 1, pp. 86–96, Feb. 2015.

[2] C. A. Fowler, "Old radar types never die, they just phased array or 55 years of trying to avoid mechanical scan," *IEEE Aerosp. Electron. Syst. Mag.*, vol. 13, no. 9, pp. 24A–24L, Sep. 1998.

[3] A. J. Fenn, D. H. Temme, W. P. Delaney, and W. E. Courtney, "The development of phased-array radar technology," *Lincoln Lab. J.*, vol. 12, no. 2, pp. 321–340, 2000.

[4] D. Parker and D. C. Zimmermann, "Phased arrays—Part 1: Theory and architectures," *IEEE Trans. Microw. Theory Techn.*, vol. 53, no. 2, pp. 678–687, Mar. 2002.

[5] D. Parker and D. C. Zimmermann, "Phased arrays—Part II: Implementations, applications, and future trends," *IEEE Trans. Microw. Theory Techn.*, vol. 53, no. 2, pp. 688–698, Mar. 2002.

[6] A. S. Y. Poon and M. Taghivand, "Supporting and enabling circuits for antenna arrays in wireless communications," *Proc. IEEE*, vol. 100, no. 7, pp. 2207–2218, Jul. 2012.

[7] E. Brookner, "Developments and breakthroughs in radars and phased-arrays," in *Proc. IEEE Radar Conf. (RadarConf)*, Philadelphia, PA, USA, May 2016, pp. 1–6, doi: 10.1109/RADAR.2016.7485273.

[8] D. L. Jones, "Technology challenges for the square kilometer array," *IEEE Aerosp. Electron. Syst. Mag.*, vol. 28, no. 2, pp. 18–23, Feb. 2013.

[9] P.-F. Li, S.-W. Qu, and S. Yang, "Two-dimensional imaging based on near-field focused array antenna," *IEEE Antennas Wireless Propag. Lett.*, vol. 18, no. 2, pp. 274–278, Feb. 2019.

[10] F. Roos, J. Bechter, C. Knill, B. Schweizer, and C. Waldschmidt, "Radar sensors for autonomous driving: Modulation schemes and interference mitigation," *IEEE Microw. Mag.*, vol. 20, no. 9, pp. 58–72, Sep. 2019.

[11] B. Sadhu, X. Gu, and A. Valdes-Garcia, "The more (Antennas), the merrier: A survey of silicon-based mm-wave phased arrays using multi-IC scaling," *IEEE Microw. Mag.*, vol. 20, no. 12, pp. 32–50, Dec. 2019.

[12] R. S. Elliott, *Antenna Theory and Design*. Hoboken, NJ, USA: Wiley, 2003.

[13] R. J. Mailloux, *Phased Array Antenna Handbook*, 3rd ed. Boston, MA, USA: Artech House, 2017.

[14] R. L. Haupt, *Antenna Arrays: A Computational Approach*. New York, NY, USA: Wiley, 2010.

[15] C. Fulton, M. Yeary, D. Thompson, J. Lake, and A. Mitchell, "Digital phased arrays: Challenges and opportunities," *Proc. IEEE*, vol. 104, no. 3, pp. 487–503, Mar. 2016.

[16] J. S. Herd and M. D. Conway, "The evolution to modern phased array architectures," *Proc. IEEE*, vol. 104, no. 3, pp. 519–529, Mar. 2016.

[17] S. H. Talisa, K. W. O'Haver, T. M. Comberiate, M. D. Sharp, and O. F. Somerlock, "Benefits of digital phased array radars," *Proc. IEEE*, vol. 104, no. 3, pp. 530–543, Mar. 2016.

[18] C. Fulton, R. Palmer, M. Yeary, J. Salazar, H. Sigmarsson, M. Weber, and A. Hedden, "Horus: A testbed for fully digital phased array radars," *Microw. J.*, vol. 63, no. 1, pp. 20–36, Jan. 2020.

[19] M. Yeary, R. Palmer, C. Fulton, J. Salazar, and H. Sigmarsson, "Recent advances on an S-band all-digital mobile phased array radar," in *Proc. IEEE Int. Symp. Phased Array Syst. Technol. (PAST)*, Waltham, MA, USA, Oct. 2019, pp. 1–5, doi: 10.1109/PAST43306.2019.9020988.

[20] M. Yeary, D. Conway, J. Herd, M. Fosberry, M. Harger, and K. Hondl, "A least mean squares approach of iterative array calibration for scalable digital phased array radar panels," in *Proc. IEEE Int. Symp. Phased Array Syst. Technol.*, Waltham, MA, USA, Oct. 2013, pp. 276–278, doi: 10.1109/ARRAY.2013.6731841.

[21] R. Lebron, J. Diaz, and J. Salazar-Cerreno, "A procedure to characterize and predict active phased array antenna radiation patterns from planar near-field measurements," in *Proc. AMTA*, Williamsburg, VA, USA, 2018, pp. 1–4.

[22] A. Dreher, N. Niklasch, F. Klefenz, and A. Schroth, "Antenna and receiver system with digital beamforming for satellite navigation and communications," *IEEE Trans. Microw. Theory Techn.*, vol. 51, no. 7, pp. 1815–1821, Jul. 2003.

[23] M. Joler, "How FPGAs can help create self-recoverable antenna arrays," *Int. J. Antennas Propag.*, vol. 2012, Jan. 2012, Art. no. 196925, doi: 10.1155/2012/196925.

[24] J. Ruze, "The effect of aperture errors on the antenna radiation pattern," *Il Nuovo Cimento*, vol. 9, no. S3, pp. 364–380, Mar. 1952.

[25] J. K. Hsiao, "Design of error tolerance of a phased array," *Electron. Lett.*, vol. 21, no. 19, pp. 834–836, Sep. 1985.

[26] J. Lee, Y. Lee, and H. Kim, "Decision of error tolerance in array element by the Monte Carlo method," *IEEE Trans. Antennas Propag.*, vol. 53, no. 4, pp. 1325–1331, Apr. 2005.

[27] A. J. van den Biggelaar, U. Johannsen, P. Mattheijssen, and A. B. Smolders, "Improved statistical model on the effect of random errors in the phase and amplitude of element excitations on the array radiation pattern," *IEEE Trans. Antennas Propag.*, vol. 66, no. 5, pp. 2309–2317, May 2018.

[28] E. L. Holzman, "A different perspective on taper efficiency for array antennas," *IEEE Trans. Antennas Propag.*, vol. 51, no. 10, pp. 2963–2967, Oct. 2003.

[29] Arun K. Bhattacharyya, *Phased Array Antennas, Floquet Analysis, Synthesis, BFNs and Active Array Systems*. Hoboken, NJ, USA: Wiley, 2006.

[30] P. Rocca, L. Manica, N. Anselmi, and A. Massa, "Analysis of the pattern tolerances in linear arrays with arbitrary amplitude errors," *IEEE Antennas Wireless Propag. Lett.*, vol. 12, pp. 639–642, Dec. 2013.

[31] N. Anselmi, L. Manica, P. Rocca, and A. Massa, "Tolerance analysis of antenna arrays through interval arithmetic," *IEEE Trans. Antennas Propag.*, vol. 61, no. 11, pp. 5496–5507, Nov. 2013.

[32] N. Anselmi, P. Rocca, M. Salucci, and A. Massa, "Optimisation of excitation tolerances for robust beamforming in linear arrays," *IET Microw., Antennas Propag.*, vol. 10, no. 2, pp. 208–214, Jan. 2016.

[33] N. Anselmi, P. Rocca, M. Salucci, and A. Massa, "Power pattern sensitivity to calibration errors and mutual coupling in linear arrays through circular interval arithmetics," *Sensors*, vol. 16, no. 6, pp. 1–14, 2016.

[34] A. Massa, P. Rocca, E. Giaccari, and A. Farina, "Tolerance analysis of antenna arrays through interval analysis," in *Proc. IEEE Radar Conf.*, Cincinnati, OH, USA, May 2014, pp. 0896–0899, doi: 10.1109/RADAR.2014.6875718.

[35] N. Anselmi, M. A. Hannan, and P. Rocca, "Optimal synthesis of maximally robust antenna arrays by means of circular interval arithmetics," in *Proc. IEEE Int. Symp. Antennas Propag. USNC-URSI Radio Sci. Meeting*, Atlanta, GA, USA, Jul. 2019, pp. 749–750, doi: 10.1109/APUSNCURSINRSM.2019.8888575.

[36] L. Tenuti, N. Anselmi, P. Rocca, M. Salucci, and A. Massa, "Minkowski sum method for planar arrays sensitivity analysis with uncertain-but-bounded excitation tolerances," *IEEE Trans. Antennas Propag.*, vol. 65, no. 1, pp. 167–177, Jan. 2017.

[37] G. He, X. Gao, H. Zhou, and H. Zhu, "Comparison of three interval arithmetic-based algorithms for antenna array pattern upper bound estimation," *Electron. Lett.*, vol. 55, no. 14, pp. 775–776, Jul. 2019.

[38] G. He, X. Gao, and H. Zhou, "Matrix-based interval arithmetic for linear array tolerance analysis with excitation amplitude errors," *IEEE Trans. Antennas Propag.*, vol. 67, no. 5, pp. 3516–3520, May 2019.

[39] M. de Berg, O. Cheong, M. van Kreveld, and M. Overmars, *Computational Geometry Algorithms and Applications*, 3rd ed. Berlin, Germany: Springer-Verlag, 2008, ch. 13, p. 297.

[40] P. Rocca, N. Anselmi, A. Benoni, and A. Massa, "Probabilistic interval analysis for the analytic prediction of the pattern tolerance distribution in linear phased arrays with random excitation errors," *IEEE Trans. Antennas Propag.*, vol. 68, no. 12, pp. 7866–7878, Dec. 2020.

[41] I. Seker, "Calibration methods for phased array radars," *Proc. SPIE*, vol. 8714, pp. 1–15, May 2013.

[42] C. Fulton, "Digital array radar calibration and performance monitoring techniques, including direct conversion and dual polarization architectures," Ph.D. dissertation, Dept. Elect. Comput. Eng., Purdue Univ., West Lafayette, IN, USA, 2011.

[43] D. Hess, A. Fenn, D. Garneski, and C. Kryzak, "Phased array antenna measurements tutorial session," in *Proc. IEEE Int. Symp. Tutorial Session*, Waltham, MA, USA, Oct. 2010.

[44] W. T. Patton and L. H. Yorinks, "Near-field alignment of phased-array antennas," *IEEE Trans. Antennas Propag.*, vol. 47, no. 3, pp. 584–591, Mar. 1999.

[45] K. Hassett, "Phased array antenna calibration measurement techniques and methods," in *Proc. Eur. Conf. Antennas Propag.*, 2016, pp. 1–4.

[46] A. Stark, B. Rohrdantz, U. Johannsen, and A. F. Jacob, "*In-situ* probes for patch antenna array calibration," *Int. J. Microw. Wireless Tech.*, vol. 3, no. 3, pp. 273–280, 2011.

[47] Y. V. Korotetskiy, A. M. Shitikov, and V. V. Denisenko, "Phased array antenna calibration with probe positioning errors [Measurements Corner]," *IEEE Antennas Propag. Mag.*, vol. 58, no. 3, pp. 65–80, Jun. 2016.

[48] J. K. Mulcahey and M. G. Sarcione, "Calibration and diagnostics of the THAAD solid state phased array in a planar nearfield facility," in *Proc. Int. Symp. Phased Array Syst. Technol.*, Boston, MA, USA, 1996, pp. 322–326, doi: 10.1109/PAST.1996.566108.

[49] M. Sarcione, J. Mulcahey, D. Schmidt, K. Chang, M. Russell, R. Enzmann, P. Rawlinson, W. Guzak, R. Howard, and M. Mitchell, "The design, development and testing of the THAAD (Theater high altitude area Defense) solid state phased array (formerly ground based radar)," in *Proc. Int. Symp. Phased Array Syst. Technol.*, Boston, MA, USA, 1996, pp. 260–265, doi: 10.1109/PAST.1996.566096.

[50] A. Agrawal and A. Jablon, "A calibration technique for active phased array antennas," in *Proc. IEEE Int. Symp. Phased Array Syst. Technol.*, Boston, MA, USA, Oct. 2003, pp. 223–228, doi: 10.1109/PAST.2003.1256985.

[51] J.-J. Nicolas, "*In situ* array antenna diagnosis using microwave circular holography," in *Proc. IEEE Int. Symp. Phased Array Syst. Technol.*, Waltham, MA, USA, Oct. 2010, pp. 298–305, doi: 10.1109/ARRAY.2010.5613353.

[52] H. Pawlak, A. Charaspreedalarp, and A. Jacob, "Experimental investigation of an external calibration scheme for 30 GHz circularly polarized DBF transmit antenna arrays," in *Proc. Eur. Microw. Conf.*, Manchester, U.K., Sep. 2006, pp. 764–767, doi: 10.1109/EUMC.2006.281031.

[53] C. Fulton, J. L. Salazar, Y. Zhang, G. Zhang, R. Kelly, J. Meier, M. McCord, D. Schmidt, A. D. Byrd, L. M. Bhowmik, S. Karimkashi, D. S. Zrnic, R. J. Doviak, A. Zahrai, M. Yeary, and R. D. Palmer, "Cylindrical polarimetric phased array radar: Beamforming and calibration for weather applications," *IEEE Trans. Geosci. Remote Sens.*, vol. 55, no. 5, pp. 2827–2841, May 2017.

[54] B. Rousta, M. Naser-Moghadasi, B. A. Arand, and R. A. Sadeghzadeh, "An efficient scheduling for fast calibration of digital beamforming active phased array radar," *IETE J. Res.*, early access, pp. 1–7, Aug. 2019, doi: 10.1080/03772063.2019.1610513.

[55] M. Fernandez, Y. Lopez, and L. Fernando, "Dual-probe near-field phaseless antenna measurement system on board a UAV," *Sensors*, vol. 19, no. 21, pp. 1–18, 2019.

[56] M. Garcia-Fernandez, Y. A. Lopez, and F. L. Andres, "Unmanned aerial system for antenna measurement and diagnosis: Evaluation and testing," *IET Microw., Antennas Propag.*, vol. 13, no. 13, pp. 2224–2231, Oct. 2019.

[57] H. Pawlak and A. F. Jacob, "An external calibration scheme for DBF antenna arrays," *IEEE Trans. Antennas Propag.*, vol. 58, no. 1, pp. 59–67, Jan. 2010.

[58] T. Takahashi, N. Nakamoto, M. Ohtsuka, T. Aoki, Y. Konishi, I. Chiba, and M. Yajima, "On-board calibration methods for mechanical distortions of satellite phased array antennas," *IEEE Trans. Antennas Propag.*, vol. 60, no. 3, pp. 1362–1372, Mar. 2012.

[59] J. A. Haimerl, B. Hudson, G. P. Fonder, and D. K. Lee, "Overview of the large digital arrays of the space fence radar," in *Proc. IEEE Int. Symp. Phased Array Syst. Technol. (PAST)*, Waltham, MA, USA, Oct. 2016, pp. 1–8, doi: 10.1109/ARRAY.2016.7832538.

[60] M. Scott, "SAMPSON MFR active phased array antenna," in *Proc. IEEE Int. Symp. Phased Array Syst. Technol.*, Boston, MA, USA, Oct. 2003, pp. 119–123, doi: 10.1109/PAST.2003.1256967.

[61] H. M. Aumann, A. J. Fenn, and F. G. Willwerth, "Phased array antenna calibration and pattern prediction using mutual coupling measurements," *IEEE Trans. Antennas Propag.*, vol. 37, no. 7, pp. 844–850, Jul. 1989.

[62] G. F. Lewis and E. Boe, "Self-phase up of array antennas with non-uniform element mutual coupling and arbitrary lattice orientation," U.S. Patent 5 657 023, Aug. 12, 1997.

[63] C. Shipley and D. Woods, "Mutual coupling-based calibration of phased array antennas," in *Proc. IEEE Int. Conf. Phased Array Syst. Technol.*, Dana Point, CA, USA, May 2000, pp. 529–532, doi: 10.1109/PAST.2000.859012.

[64] T. Gao, J. Wang, Y. Guo, and X. Chen, "Large phased array antenna calibration using mutual coupling method," in *Proc. CIE Int. Conf. Radar*, Beijing, China, 2001, pp. 223–226, doi: 10.1109/ICR.2001.984660.

[65] M. A. S. Natera, R. M. Rodriguez-Osorio, L. de Haro Ariet, and M. S. Perez, "Calibration proposal for new antenna array architectures and technologies for space communications," *IEEE Antennas Wireless Propag. Lett.*, vol. 11, pp. 1129–1132, Aug. 2012, doi: 10.1109/LAWP.2012.2215952.

[66] Y. Neidman, R. Shavit, and A. Bronshtein, "Diagnostic of phased arrays with faulty elements using the mutual coupling method," *IET Microw., Antennas Propag.*, vol. 3, no. 2, pp. 235–241, Mar. 2009.

[67] C. Fulton and W. Chappell, "Calibration techniques for digital phased arrays," in *Proc. IEEE Int. Conf. Microw., Commun., Antennas Electron. Syst.*, Tel Aviv, Israel, Nov. 2009, pp. 1–10, doi: 10.1109/COMCAS.2009.5385979.

[68] F. S. Gerino and P. M. Belcaguy, "Mutual coupling internal calibration method applied to a polarimetric phased array antenna model," in *Proc. IEEE Global Electromagn. Compat. Conf. (GEMCCON)*, Mar del Plata, Argentina, Nov. 2016, pp. 1–5, doi: 10.1109/GEMCCON.2016.7797310.

[69] D. Bekers, R. van Dijk, and F. van Vliet, "Mutual-coupling based phased-array calibration: A robust and versatile approach," in *Proc. IEEE Int. Symp. Phased Array Syst. Technol.*, Waltham, MA, USA, Oct. 2013, pp. 630–637, doi: 10.1109/ARRAY.2013.6731903.

[70] R. M. Lebron, P.-S. Tsai, J. M. Emmett, C. Fulton, and J. L. Salazar-Cerreno, "Validation and testing of initial and *in-situ* mutual coupling-based calibration of a dual-polarized active phased array antenna," *IEEE Access*, vol. 8, pp. 78315–78329, 2020.

[71] J. Lujan, C. J. Fulton, M. Yeary, E. A. Langley, S. McCormick, and A. Hedden, "Phased array radar initial alignment algorithm using mutual coupling: An iterative approach," *Proc. SPIE*, vol. 11408, Apr. 2020, Art. no. 1140811.

[72] J. Herd, "Experimental results from a self-calibrating digital beamforming array," in *Proc. Int. Symp. Antennas Propag. Soc., Merging Technol.*, Dallas, TX, USA, 1990, pp. 384–387, doi: 10.1109/APS.1990.115127.

[73] O. Inac, S. Y. Kim, D. Shin, C. Y. Kim, and G. M. Rebeiz, "Built-in self test systems for silicon-based phased arrays," in *IEEE MTT-S Int. Microw. Symp. Dig.*, Montreal, QC, Canada, Jun. 2012, pp. 1–3, doi: 10.1109/MWSYM.2012.6259455.

[74] D. Kissinger, B. Laemmle, L. Maurer, and R. Weigel, "Integrated test for silicon front ends," *IEEE Microw. Mag.*, vol. 11, no. 3, pp. 87–94, May 2010.

[75] D. Kissinger, R. Agethen, and R. Weigel, "A versatile built-in test architecture for integrated millimeter-wave radar receiver front-ends," in *Proc. IEEE Int. Instrum. Meas. Technol. Conf.*, Graz, Austria, May 2012, pp. 254–258, doi: 10.1109/I2MTC.2012.6229244.

[76] X. Gu, A. Valdes-Garcia, A. Natarajan, B. Sadhu, D. Liu, and S. K. Reynolds, "W-band scalable phased arrays for imaging and communications," *IEEE Commun. Mag.*, vol. 53, no. 4, pp. 196–204, Apr. 2015.

[77] K.-M. Lee, R.-S. Chu, and S.-C. Liu, "A built-in performance-monitoring/fault isolation and correction (PM/FIC) system for active phased-array antennas," *IEEE Trans. Antennas Propag.*, vol. 41, no. 11, pp. 1530–1540, Nov. 1993.

[78] A. Valdes-Garcia, B. Floyd, S. T. Nicolson, J.-W. Lai, A. Natarajan, P.-Y. Chen, S. K. Reynolds, J.-H.-C. Zhan, D. G. Kam, and D. Liu, "A fully integrated 16-element phased-array transmitter in SiGe BiCMOS for 60-GHz communications," *IEEE J. Solid-State Circuits*, vol. 45, no. 12, pp. 2757–2773, Dec. 2010.

[79] A. Natarajan, S. K. Reynolds, M.-D. Tsai, S. T. Nicolson, J.-H.-C. Zhan, D. G. Kam, D. Liu, Y.-L.-O. Huang, A. Valdes-Garcia, and B. A. Floyd, "A fully-integrated 16-element phased-array receiver in SiGe BiCMOS for 60-GHz communications," *IEEE J. Solid-State Circuits*, vol. 46, no. 5, pp. 1059–1075, May 2011.

[80] O. Inac, D. Shin, and G. M. Rebeiz, "A phased array RFIC with built-in self-test capabilities," *IEEE Trans. Microw. Theory Techn.*, vol. 60, no. 1, pp. 139–148, Jan. 2012.

[81] O. Inac, F. Golcuk, T. Kanar, and G. M. Rebeiz, "A 90–100-GHz phased-array transmit/receive silicon RFIC module with built-in self-test," *IEEE Trans. Microw. Theory Techn.*, vol. 61, no. 10, pp. 3774–3782, Oct. 2013.

[82] S. Young Kim, O. Inac, C.-Y. Kim, D. Shin, and G. M. Rebeiz, "A 76–84-GHz 16-element phased-array receiver with a chip-level built-in self-test system," *IEEE Trans. Microw. Theory Techn.*, vol. 61, no. 8, pp. 3083–3098, Aug. 2013.

[83] B. Brautigam, M. Schwerdt, M. Bachmann, and M. Stangl, "Individual T/R module characterisation of the TerraSAR-X active phased array antenna by calibration pulse sequences with orthogonal codes," in *Proc. IEEE Int. Geosci. Remote Sens. Symp.*, Barcelona, Spain, Jul. 2007, pp. 5202–5205, doi: 10.1109/IGARSS.2007.4424034.

[84] M. Schwerdt, M. Bachmann, D. Schrank, B. During, B. Braautigam, J. H. Gonzalez, and C. Schulz, "Precise calibration techniques for complex SAR systems based on active phased array antennas," in *Proc. IEEE Int. Symp. Phased Array Syst. Technol.*, Waltham, MA, USA, Oct. 2010, pp. 695–699, doi: 10.1109/ARRAY.2010.5613290.

[85] D. J. Rabideau, R. J. Galejs, F. G. Willwerth, and D. S. McQueen, "An S-band digital array radar testbed," in *Proc. IEEE Int. Symp. Phased Array Syst. Technol.*, Boston, MA, USA, Oct. 2003, pp. 113–118, doi: 10.1109/PAST.2003.1256966.

[86] S.-C. Chae, H.-W. Jo, J.-I. Oh, G. Kim, and J.-W. Yu, "Coupler integrated microstrip patch linear phased array for self-calibration," *IEEE Antennas Wireless Propag. Lett.*, vol. 19, no. 9, pp. 1615–1619, Sep. 2020.

[87] T. W. Nuteson, J. E. Stocker, J. S. Clark, D. S. Haque, and G. S. Mitchell, "Performance characterization of FPGA techniques for calibration and beamforming in smart antenna applications," *IEEE Trans. Microw. Theory Techn.*, vol. 50, no. 12, pp. 3043–3051, Dec. 2002.

[88] G. Liang, W. Gong, H. Liu, and J. Yu, "61-channel digital beamforming (DBF) transmitter array," in *Proc. Asia Pacific Microw. Conf.*, Singapore, Dec. 2009, pp. 739–743.

[89] G. Liang, W. Gong, H. Liu, and J. Yu, "Development of 61-channel digital beamforming (DBF) transmitter array for mobile satellite communication," *Prog. Electromagn. Res.*, vol. 97, pp. 177–195, 2009.

[90] A. M. Shitikov and A. V. Bondarik, "Multi-element PAA calibration with REV method," in *Proc. 4th Int. Conf. Antenna Theory Techn.*, Sevastopol, Ukraine, Sep. 2003, pp. 761–764.

[91] S. Mano and T. Katagi, "A method for measuring amplitude and phase of each radiating element of a phased array antenna," *Electron. Commun. Jpn.*, vol. 65, no. 5, pp. 58–64, 1982.

[92] T. Takahashi, H. Miyashita, Y. Konishi, and S. Makino, "Theoretical study on measurement accuracy of rotating element electric field vector (REV) method," *Electron. Commun. Jpn.*, vol. 89, no. 1, pp. 22–33, Jan. 2006.

[93] T. Takahashi, Y. Konishi, and I. Chiba, "A novel amplitude-only measurement method to determine element fields in phased arrays," *IEEE Trans. Antennas Propag.*, vol. 60, no. 7, pp. 3222–3230, Jul. 2012.

[94] R. Sorace, "Phased array calibration," *IEEE Trans. Antennas Propag.*, vol. 49, no. 4, pp. 517–525, Apr. 2001.

[95] R. Long, J. Ouyang, F. Yang, W. Han, and L. Zhou, "Fast amplitude-only measurement method for phased array calibration," *IEEE Trans. Antennas Propag.*, vol. 65, no. 4, pp. 1815–1822, Apr. 2017.

[96] G. He, X. Gao, and H. Zhou, "Fast phased array calibration by power-only measurements twice for each antenna element," *Int. J. Antennas Propag.*, vol. 2019, Apr. 2019, Art. no. 6432149.

[97] S. B. Sleiman, A. Akour, W. Khalil, and M. Ismail, "Millimeter-wave BiST and BiSC using a high-definition sub-ranged detector in 90 nm CMOS," in *Proc. 53rd IEEE Int. Midwest Symp. Circuits Syst.*, Seattle, WA, USA, Aug. 2010, pp. 477–480, doi: 10.1109/MWSCAS.2010.5548737.

[98] Y. Takeda, T. Fujibayashi, Y.-S. Yeh, W. Wang, and B. Floyd, "A 76− to 81-GHz transceiver chipset for long-range and short-range automotive radar," in *IEEE MTT-S Int. Microw. Symp. Dig.*, Tampa, FL, USA, Jun. 2014, pp. 1–3, doi: 10.1109/MWSYM.2014.6848490.

[99] E. Cohen, M. Ruberto, M. Cohen, O. Degani, S. Ravid, and D. Ritter, "A CMOS bidirectional 32-element phased-array transceiver at 60 GHz with LTCC antenna," *IEEE Trans. Microw. Theory Techn.*, vol. 61, no. 3, pp. 1359–1375, Mar. 2013.

[100] R. Long, J. Ouyang, F. Yang, Y. Li, K. Zhang, and L. Zhou, "Calibration method of phased array based on near-field measurement system," in *Proc. IEEE Antennas Propag. Soc. Int. Symp. (APSURSI)*, Memphis, TN, USA, Jul. 2014, pp. 1161–1162, doi: 10.1109/APS.2014.6904907.

[101] S. D. Silverstein, "Application of orthogonal codes to the calibration of active phased array antennas for communication satellites," *IEEE Trans. Signal Process.*, vol. 45, no. 1, pp. 206–218, Jan. 1997.

[102] E. Lier, M. Zemlyansky, D. Purdy, and D. Farina, "Phased array calibration and characterization based on orthogonal coding: Theory and experimental validation," in *Proc. IEEE Int. Symp. Phased Array Syst. Technol.*, Waltham, MA, USA, Oct. 2010, pp. 271–278, doi: 10.1109/ARRAY.2010.5613357.

[103] Y. Lin, X. Bu, W. Zhao, and S. Wang, "Parallel calibration method for phased array antennas with orthogonal and nonorthogonal codes," in *Proc. 10th Int. Conf. Commun. Netw. China (ChinaCom)*, Shanghai, China, Aug. 2015, pp. 883–886, doi: 10.1109/CHINACOM.2015.7498062.

[104] Y. Lin, S. Wang, X. Bu, C. Xing, and J. An, "NOMA-based calibration for large-scale spaceborne antenna arrays," *IEEE Trans. Veh. Technol.*, vol. 67, no. 3, pp. 2231–2242, Mar. 2018.

[105] G. H. C. Van Werkhaven and A. K. Golshayan, "Calibration aspects of the APAR antenna unit," in *Proc. IEEE Int. Conf. Phased Array Syst. Technol.*, Dana Point, CA, USA, May 2000, pp. 425–428, doi: 10.1109/PAST.2000.858989.

[106] M. Bachmann, M. Schwerdt, and B. Brautigam, "TerraSAR-X antenna calibration and monitoring based on a precise antenna model," *IEEE Trans. Geosci. Remote Sens.*, vol. 48, no. 2, pp. 690–701, Feb. 2010.

[107] M. Schwerdt, K. Schmidt, N. T. Ramon, P. Klenk, N. Yague-Martinez, P. Prats-Iraola, M. Zink, and D. Geudtner, "Independent system calibration of sentinel-1B," *Remote Sens.*, vol. 9, no. 511, pp. 1–34, 2017.

[108] R. Long, J. Ouyang, F. Yang, W. Han, and L. Zhou, "Multi-element phased array calibration method by solving linear equations," *IEEE Trans. Antennas Propag.*, vol. 65, no. 6, pp. 2931–2939, Jun. 2017.

[109] G. A. Hampson and A. B. Smolders, "A fast and accurate scheme for calibration of active phased-array antennas," in *IEEE Antennas Propag. Soc. Int. Symp. Dig. Held Conjunct, USNC/URSI Nat. Radio Sci. Meeting*, Orlando, FL, USA, Jul. 1999, pp. 1040–1043, doi: 10.1109/APS.1999.789490.

[110] B. Smolders and G. Hampson, "Deterministic RF nulling in phased arrays for the next generation of radio telescopes," *IEEE Antennas Propag. Mag.*, vol. 44, no. 4, pp. 13–22, Aug. 2002.

[111] T. Takahashi, Y. Konishi, S. Makino, H. Ohmine, and H. Nakaguro, "Fast measurement technique for phased array calibration," *IEEE Trans. Antennas Propag.*, vol. 56, no. 7, pp. 1888–1899, Jul. 2008.

[112] C. He, X. Liang, J. Geng, and R. Jin, "Parallel calibration method for phased array with harmonic characteristic analysis," *IEEE Trans. Antennas Propag.*, vol. 62, no. 10, pp. 5029–5036, Oct. 2014.

[113] K. Greene, V. Chauhan, and B. Floyd, "Built-in test of phased arrays using code-modulated interferometry," *IEEE Trans. Microw. Theory Techn.*, vol. 66, no. 5, pp. 2463–2479, May 2018.

[114] K. Greene, V. Chauhan, and B. Floyd, "Code-modulated embedded test for phased arrays," in *Proc. IEEE 34th VLSI Test Symp. (VTS)*, Las Vegas, NV, USA, Apr. 2016, pp. 1–4.

[115] H. S. C. Wang, "Performance of phased-array antennas with mechanical errors," *IEEE Trans. Aerosp. Electron. Syst.*, vol. 28, no. 2, pp. 535–545, Apr. 1992.

[116] C. Wang, M. Kang, W. Wang, J. Zhong, Y. Zhang, C. Jiang, and B. Duan, "Electromechanical coupling based performance evaluation of distorted phased array antennas with random position errors," *Int. J. Appl. Electromagn. Mech.*, vol. 51, no. 3, pp. 285–295, Jul. 2016.

[117] C. Wang, M. Kang, W. Wang, B. Duan, L. Lin, and L. Ping, "On the performance of array antennas with mechanical distortion errors considering element numbers," *Int. J. Electron.*, vol. 104, no. 3, pp. 462–484, Mar. 2017.

[118] C. Wang, Y. Wang, X. Yang, W. Gao, C. Jiang, L. Wang, Y. Zhang, and M. Wang, "Effect of randomness in element position on performance of communication array antennas in Internet of Things," *Wireless Commun. Mobile Comput.*, vol. 2018, Mar. 2018, Art. no. 6492143.

[119] F. Guo, Z. Liu, G. Sa, and J. Tan, "A position error representation method for planar arrays," *IEEE Antennas Wireless Propag. Lett.*, vol. 19, no. 1, pp. 109–113, Jan. 2020.

[120] C. Wang, S. Yuan, W. Gao, C. Jiang, C. Zhu, P. Li, Z. Wang, X. Peng, and Y. Shi, "A Taylor-surrogate-model-based method for the electrical performance of array antennas under interval position errors," *IEEE Antennas Wireless Propag. Lett.*, vol. 19, no. 7, pp. 1221–1225, Jul. 2020.

[121] T. H. Ismail and Z. M. Hamici, "Array pattern synthesis using digital phase control by quantized particle swarm optimization," *IEEE Trans. Antennas Propag.*, vol. 58, no. 6, pp. 2142–2145, Jun. 2010.

[122] W. P. M. N. Keizer, "Low sidelobe phased array pattern synthesis with compensation for errors due to quantized tapering," *IEEE Trans. Antennas Propag.*, vol. 59, no. 12, pp. 4520–4524, Dec. 2011.

[123] M. S. Smith and Y. C. Guo, "A comparison of methods for randomizing phase quantization errors in phased arrays," *IEEE Trans. Antennas Propag.*, vol. 31, no. 6, pp. 821–827, Nov. 1983.

[124] R. L. Haupt, "Antenna arrays in the time domain: An introduction to timed arrays," *IEEE Antennas Propag. Mag.*, vol. 59, no. 3, pp. 33–41, Jun. 2017, doi: 10.1109/MAP.2017.2686082.

[125] R. L. Haupt and P. Nayeri, "Pulse dispersion in phased arrays," *Int. J. Antennas Propag.*, vol. 2017, Apr. 2017, Art. no. 5717641, doi: 10.1155/2017/5717641.

[126] J. B. Thomas, "The tone generator and phase calibration in VLBI measurements," Jet Propuls. Lab., Pasadena, CA, USA, Deep Space Netw. Prog. Rep. 42-44, Apr. 1978, pp. 63–74.

[127] C. S. Jacobs, "Phase calibration tone processing with the block II VLBI correlator," Jet Propuls. Lab., Pasadena, CA, USA, TMO Prog. Rep. 42-134, Aug. 1998, pp. 1–22.

[128] R. Hamell, B. Tucker, and M. Calhoun, "Phase calibration generator," Jet Propuls. Lab., Pasadena, CA, USA, IPN Prog. Rep. 42-154, Aug. 2003, pp. 1–14.

[129] L. L. Liou, D. M. Lin, M. Longbrake, P. Buxa, J. McCann, T. Dalrymple, J. B. Tsui, R. Qiu, Z. Hu, and N. Guo, "Digital wideband phased array calibration and beamforming using time reversal technique," in *Proc. IEEE Int. Symp. Phased Array Syst. Technol.*, Waltham, MA, USA, Oct. 2010, pp. 261–266, doi: 10.1109/ARRAY.2010.5613359.

[130] A. Massa, G. Oliveri, M. Salucci, N. Anselmi, and P. Rocca, "Learning-by-examples techniques as applied to electromagnetics," *J. Electromagn. Waves Appl.*, vol. 32, no. 4, pp. 516–541, Mar. 2018, doi: 10.1080/09205071.2017.1402713.

[131] L. Li, L. G. Wang, F. L. Teixeira, C. Liu, A. Nehorai, and T. J. Cui, "DeepNIS: Deep neural network for nonlinear electromagnetic inverse scattering," *IEEE Trans. Antennas Propag.*, vol. 67, no. 3, pp. 1819–1825, Mar. 2019.

[132] A. Massa, D. Marcantonio, X. Chen, M. Li, and M. Salucci, "DNNs as applied to electromagnetics, antennas, and propagation—A review," *IEEE Antennas Wireless Propag. Lett.*, vol. 18, no. 11, pp. 2225–2229, Nov. 2019.

[133] S. D. Campbell, R. P. Jenkins, P. J. O'Connor, and D. H. Werner, "The explosion of artificial intelligence in antennas and propagation: How deep learning is advancing our state of the art," *IEEE Antennas Propag. Mag.*, early access, Oct. 2, 2020, doi: 10.1109/MAP.2020.3021433.

[134] F. Zardi, P. Nayeri, P. Rocca, and R. L. Haupt, "Artificial intelligence for adaptive and reconfigurable antenna arrays: A review," *IEEE Antennas Propag. Mag.*, early access, Dec. 3, 2020, doi: 10.1109/MAP.2020.3036097.

[135] L. Yang, R. Dang, M. Li, K. Zhao, C. Song, and Z. Xu, "A fast calibration method for phased arrays by using the graph coloring theory," *Sensors*, vol. 18, no. 12, pp. 1–19, 2018, doi: 10.3390/s18124315.

[136] G. Babur, D. Caratelli, and A. Mirmanov, "Phased array calibration by binary compressed sensing," *Prog. Electromagn. Res. M*, vol. 73, pp. 61–70, 2018.

[137] C. Shan, X. Chen, H. Yin, W. Wang, G. Wei, and Y. Zhang, "Diagnosis of calibration state for massive antenna array via deep learning," *IEEE Wireless Commun. Lett.*, vol. 8, no. 5, pp. 1431–1434, Oct. 2019, doi: 10.1109/LWC.2019.2920818.

GUOLONG HE received the B.S. degree in electronic engineering from Shanghai Jiao Tong University, Shanghai, China, in 2008, and the Ph.D. degree in aerospace engineering from Tsinghua University, Beijing, China, in 2016. Since 2008, he has been with the Beijing Institute of Tracking and Telecommunication Technology, Beijing, and involved in the design, construction, and maintenance of the Chinese. He is in charge of several projects with both parabolic antennas and phased array antennas. He is currently the Project Manager of 4 × 35-m deep space antenna array with the Kashi Deep Space Station. His research interests include design of satellite communication and navigation systems, and phased array signal processing.

XIN GAO received the B.S. degree in electronic engineering from Northwest University, Xi'an, China, in 1995, the M.S. degree in optics engineering from Northwestern Polytechnical University, Xi'an, in 1998, and the Ph.D. degree in optics engineering from Xi'an Institute of Optics and Precision Mechanics, Chinese Academy of Sciences, Xi'an, in 2007. He is currently a Full Professor with the Beijing Institute of Tracking and Telecommunication Technology, Beijing, China. His research interests include design of satellite communication and navigation systems, and phased array signal processing.

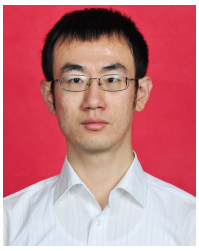

RENTIAN ZHANG received the B.S. degree in electronic engineering from the Huazhong University of Science and Technology, Wuhan, China, in 2009, and the M.S. degree in electronic engineering from Beihang University, Beijing, China, in 2011. He is currently an Assistant Professor with the Beijing Institute of Tracking and Telecommunication Technology, Beijing. His research interests include design of satellite communication and navigation systems, and phased array signal processing.